

# Establishing structure–property linkages for wicking time predictions in porous polymeric membranes using a data-driven approach

Willfried Kunz<sup>a,b,\*</sup>, Patrick Altschuh<sup>a,b,1</sup>, Marcel Bremerich<sup>d</sup>, Michael Selzer<sup>a,c</sup>, Britta Nestler<sup>a,b,c</sup>

<sup>a</sup> Institute of Digital Materials Science, Karlsruhe University of Applied Sciences, Moltkestraße 30, 76133 Karlsruhe, Germany

<sup>b</sup> Institute for Applied Materials - Microstructure Modelling and Simulation, Karlsruhe Institute of Technology (KIT), Strasse am Forum 7, 76131 Karlsruhe, Germany

<sup>c</sup> Institute of Nanotechnology, Karlsruhe Institute of Technology (KIT), Hermann-von-Helmholtz-Platz 1, 76344 Eggenstein-Leopoldshafen, Germany

<sup>d</sup> Sartorius Stedim Biotech GmbH, August-Spindler-Strasse 11, 37079 Goettingen, Germany

## ARTICLE INFO

Dataset link: <https://doi.org/10.5281/zenodo.7220573>

### Keywords:

Structure–property linkage  
Workflows  
Paper-based microfluidics  
Lateral flow assay  
High-throughput research

## ABSTRACT

The goal of this study is to develop correlations between microstructure morphology and macroscopic material behavior, known as structure–property linkages. These correlations can be used to predict material behavior and enable virtual materials design efforts. In this work the structure–property linkages for the capillary-driven fluid transport through highly porous open-pored polymeric membranes are determined by a data-driven approach. To establish linkages, about 400 porous microstructures with different geometrical features are algorithmically generated and characterized in 3D, using fluid flow simulations and image analysis methods. The data processing pipeline for the generation and analysis of the microstructures is implemented by a generic workflow tool called KadiStudio, which is embedded in the research data infrastructure Kadi4mat. The data-driven analysis enables predictions about the propagation time of a fluid over definable distances when only the porosity and the ligament radius are known as microstructural properties. The generated knowledge can be utilized for an accelerated development of novel polymeric membranes with an optimized pore structure.

## 1. Introduction

The digital transformation across all fields and disciplines is fueled by the ever-increasing computing power and new developments in data processing technologies [1] while the amount of data increased tremendously over the recent years. In consequence, the availability of huge data quantities generated by experiments or simulations has ushered in a new era based on data-driven science, commonly referred to as the fourth paradigm of science [2]. This poses new challenges for science, such as data analysis, data management, and data sharing [3]. At the same time, new opportunities are emerging to gain new insights by finding individual relationships within and between data sets.

Materials science usually deals with complex multiscale and multiphysics materials, where the different scales, e.g., atomistic, microstructural, and application scales, are usually studied in a decoupled manner by theoretical, experimental, and computational research groups [4]. The current research paradigm aims to unify the research activities

by examining and processing data from different scales and disciplines. In this way, knowledge is generated about how the process history of the material (e.g. chemical composition, thermal condition) causes the morphology of the microstructure (e.g. pore sizes and shapes) and ultimately results in a specific material behavior. These so-called process-structure-property (PSP) relationships can be based on two types of models: (i) forward models used for predictive analysis, based on cause–effect relationships (see Fig. 1), and (ii) inverse models used for optimization and design, based on goals and means relationships [2]. A concrete example of a forward model for structure–property relationships is the empirical fitting of classical fluid mechanics models such as the Kozeny–Carman equation to experimentally or computationally obtained data [5]. To accelerate the quantification and understanding of the PSP relationships, high-throughput experiments and high-throughput computing offer an excellent potential [6].

\* Corresponding author at: Institute for Applied Materials - Microstructure Modelling and Simulation, Karlsruhe Institute of Technology (KIT), Strasse am Forum 7, 76131 Karlsruhe, Germany.

E-mail addresses: [willfried.kunz@h-ka.de](mailto:willfried.kunz@h-ka.de) (W. Kunz), [patrick.altschuh@h-ka.de](mailto:patrick.altschuh@h-ka.de) (P. Altschuh), [marcel.bremerich@sartorius.com](mailto:marcel.bremerich@sartorius.com) (M. Bremerich), [michael.selzer@kit.edu](mailto:michael.selzer@kit.edu) (M. Selzer), [britta.nestler@kit.edu](mailto:britta.nestler@kit.edu) (B. Nestler).

<sup>1</sup> Equal contribution.

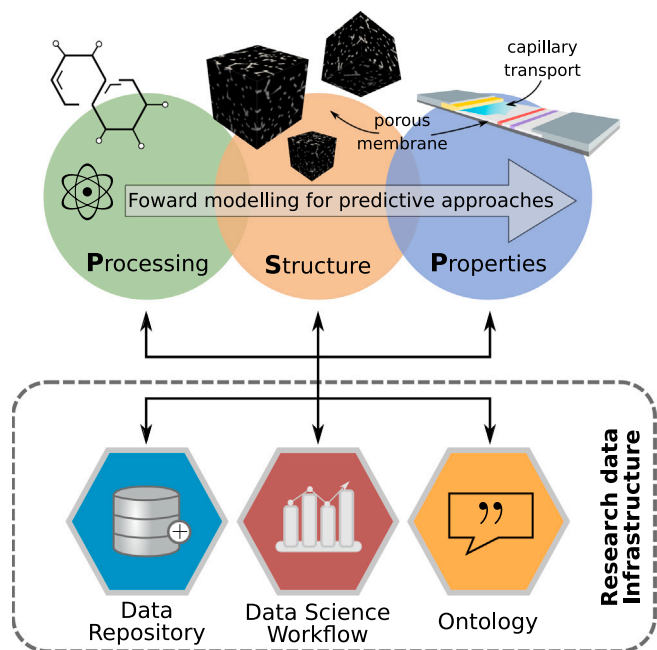


Fig. 1. The interplay between processing-structure-property relationships and the research data infrastructure. An example of forward modelling for predictive approaches.

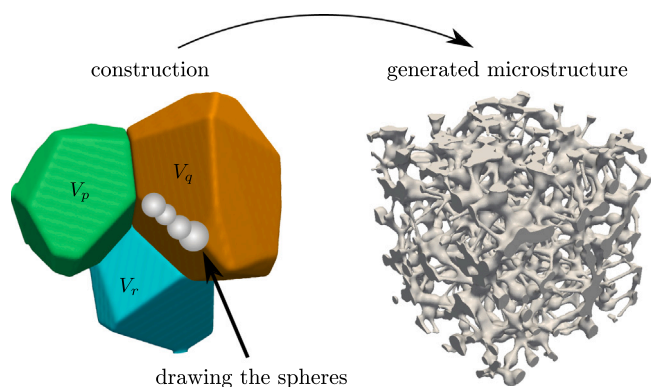


Fig. 2. Generation of a porous membrane, based on Voronoi tessellation. The left figure shows the Voronoi cells that are build on the Voronoi points  $V_p$ ,  $V_q$ , and  $V_r$  (based on [13]). Additionally, along the intersecting edges of the Voronoi cells, the drawn membrane structure is illustrated. The right figure represents the isovolume of a generated microstructure, in which the gray part represents the membrane structure.

High-throughput research activities are characterized by an automated process that enables rapid and cost-effective investigations [7]. In computational materials science in particular, high-throughput simulations are used to efficiently build an extensive database of characteristic material parameters and structural properties that form the basis for PSP linkages [8,9]. In the context of data-driven research, data infrastructures are needed that enable both the curation of data and the creation of data pipelines, so-called (data science) workflows. The latter aims at realizing preprocessing, analysis, and postprocessing tasks in an automatable, reproducible, and traceable way, thus establishing data provenance relationships. Combining data repository and data science workflows in a research data infrastructure (see Fig. 1) also incorporates the FAIR data principles [10]. Through the integration of the *KadiStudio* workflow editor [11], the Karlsruhe Data Infrastructure for material Science (*Kadi4mat*) [12] enables an excellent opportunity to realize the previous mentioned points.

This work deals with the establishment of a structure-property relationship for porous polymer membranes (PPMs). In the last decades,

PPMs have gained increasing interest. This is not least due to new application areas which could be opened up by the advantageous properties of PPMs or which would not have been feasible with alternative materials from a technical and economic point of view. The success story is based on the controlled introduction of pores into a dense polymer matrix (e.g. polymer solution), which allows the formation of thin, porous layers with unique structural properties [14–16]. Porous structures are generally defined by a material matrix, i.e. by the coherent solid that forms the actual structure, and by the pore space, which is described by pores and pore throats. For a better description of the different structural morphologies, the pore types can be further divided into isolated pores, dead-end pores and interconnected pores [17]. Depending on the combination of the different pore types, open-pored or closed-pored morphologies result. In open-pored structures, the pores are interconnected, creating a pore network that is permeable to fluids. In closed-pored structures, on the other hand, isolated pores and dead-end pores predominate, which reduces the permeability to fluids, but increases the mechanical strength and thermal conductivity of suitable structural materials, which can also be exploited as very advantageous properties.

In this work, about 400 digital twins of open-pored porous polymeric membranes, which are preferentially used in lateral flow assays (LFA), were generated algorithmically and characterized in 3D, using fluid flow simulations and image analysis techniques. The processing of the microstructures was realized by high-throughput workflows, implemented in the *KadiStudio* workflow environment. Based on the obtained data, structure linkages were obtained by applying a curve fitting procedure with the commonly known Kozeny–Carman equation, while further parameters were linked using a linear regression approach. Finally, the resulting linkages are passed to a macroscopic wicking model [18], which allows the prediction of capillary-driven fluid propagation in PPMs, just by knowing the porosity and the ligament radius, thus allowing an accelerated design of LFAs for medical diagnostic tests. This presents an easily reproducible method for addressing the scientific question of creating structure-property relationships for porous structures.

## 2. Materials and methods

### 2.1. Generating digital representations of porous polymeric membranes (PPM)

Virtual material design thrives on the ability to create digital representations that form the basis for data-driven approaches. In general, there are three different ways to obtain 3D microstructures [19]: (i) image-based capturing and reconstruction of 3D microstructures, by real material samples [20], (ii) algorithm-based generation of microstructures [21–23], and (iii) simulation-based evolution of microstructures, by solving mathematical models of physical processes [24,25]. In this data-driven approach, the necessary database is realized through the algorithm-based generation of digital representations. The algorithm is implemented in the simulation framework *PACE3D* [26], where the generation process is generally based on two main steps [21]:

- (i) The first step is to distribute Voronoi points with a defined distribution function, the so-called seed, in space. These points are entangled in neighborhood relations that allow a Voronoi cell to be defined around each Voronoi point (see Fig. 2). Due to the planes and surfaces of the Voronoi cells, they generally represent polyhedra [27].
- (ii) In the second step, the membrane structure is drawn along the intersecting edges of the polyhedra, by means of overlapping spheres. Subsequently, they are fused together by a smoothing step and finally represent the webs of the membrane structure, as can be seen in Fig. 2.

The described generation algorithm enables the generation of porous microstructures with defined structure characteristics and is controlled by several optional input parameters. Important parameters influencing the morphology are the number  $n$  of Voronoi points, the thickness of the ligaments  $r_l$  (the radius of the placed spheres), the porosity  $\phi$  and, for statistical reasons, the seed number. The pore size of the membrane structure is indirectly defined by the number of Voronoi points placed. For example, a smaller number of Voronoi points at constant ligament thickness leads to larger pores and thus a higher porosity.

In this study, the porosity and the mean ligament radius are investigated as structural characteristics and the resulting wicking behavior as a macroscopic property. The characteristic ranges of interest are based on real membrane samples [18]. They reach from 80 % to 90 % for the porosity and 0.1  $\mu\text{m}$  to 0.9  $\mu\text{m}$  for the ligament radius. To realize the ranges of the characteristic metrics, the number of Voronoi points, the porosity, and the seed number are varied. Thereby, the microstructures are generated with a domain size of  $200 \times 200 \times 200$  voxels with an assumed resolution of 150 nm per voxel. This results in cubical microstructures with 30  $\mu\text{m}$  edge lengths.

## 2.2. Computational determination of structure characteristics

To determine the relevant structural properties, both image analysis algorithms and a numerical solution of partial differential equations are used. Furthermore, the analysis is based on the full voxel representation of the digital twins, while the applied techniques are implemented in PACE3D.

### 2.2.1. Porosity

Porosity is a very commonly used effective characteristic in the field of membrane science and serves as a structural property that is usually linked to the resulting material behavior. To determine the porosity, the voxel values  $I_b = 1$  in the whole domain are summed up as follows:

$$\phi = \frac{1}{(N_x \cdot N_y \cdot N_z)} \cdot \sum_{i=1}^{N_x} \sum_{j=1}^{N_y} \sum_{k=1}^{N_z} I_b(\mathbf{x}) = \frac{N_p}{N}, \quad (1)$$

where  $N_p$  is the number of voxels in the pore space,  $N_x$ ,  $N_y$ ,  $N_z$  are the numbers of voxels along the x, y, and z direction, and  $N$  is the total number of voxels in the domain. Fig. 4b shows an example of a section of a reconstructed porous membrane.

### 2.2.2. Pore size and ligament size

The geometric mean pore radius  $\bar{r}_c$  and the mean ligament thickness  $\bar{r}_l$  of the PPMs are referred to as structure parameters [18]. They are estimated by an image analyzing method developed and implemented in PACE3D and applied in both the pore and the structural space of the digital twins. Due to the combination of a Euclidean distance map and a thinning algorithm, the method is able to estimate the local distributions of the pore sizes and the local ligament thicknesses, as respectively shown in Fig. 4c and Fig. 4d. Subsequently, the obtained distributions are used to determine the respective mean values of the structure parameter. The characterization method is described in more detail in [20].

As pointed out in our previous work [18], the wicking process in open-pored and complex porous microstructures can be correctly predicted only if an effective pore radius is used in common macroscopic flow models, instead of the geometric pore radius. Therefore, in [18], a parametric study was performed using selected simplified structures to represent the complex microstructure of the membrane. A phase-field approach was then applied, incorporating a special wetting boundary condition to describe meniscus formation and the corresponding mean surface curvature for each structure. The main result of the study was the establishment of an analytical correlation between geometric

structure parameters and an effective capillary radius  $r_{\text{eff}}$ , using a correction factor  $F(r_l, r_c)$ :

$$r_{\text{eff}} = F(r_l, r_c) \cdot r_c. \quad (2)$$

Thus, an analytical correlation was fit to the simulation results of the simplified structures to obtain the correction factor  $F(r_l, r_c)$ :

$$F(r_l, r_c) = \frac{a}{r_l/r_c} + b, \quad (3)$$

with the values  $a = 1.98$  and  $b = 3.012$ . The derivation of the effective capillary radius was validated with experimental results [18].

### 2.2.3. Permeability

To establish a relationship between the structural metrics and the resulting permeability as material behavior, fluid flow simulations are performed in the pore space as follows: First, a pressure difference  $\Delta p$  is defined over the considered PPM layer with a thickness  $L$ , while a periodic condition is applied to the remaining boundaries. In a second step, the Stokes equations for the steady-state solution are solved with a finite-difference scheme on the equidistant voxel grid, so as to obtain the spatial velocity distribution  $\mathbf{v} = (u_x, u_y, u_z)^T$ , as shown in Fig. 4e. Finally, the permeability is determined by applying Darcy's law

$$K = \frac{\eta U L}{\Delta p}, \quad (4)$$

where  $\eta$  describes the dynamic viscosity and  $U$  denotes the Darcy velocity in the main flow direction (e.g.  $U = \phi \bar{u}_x$ ). To validate the permeability determination, analytical investigations are typically conducted using simplified porous structures. A widely used approach is the Gebart equation [28]

$$\frac{K}{r_l^2} = C \left( \sqrt{\frac{1 - \phi_c}{1 - \phi}} - 1 \right)^{\frac{5}{2}}, \quad (5)$$

here  $\phi_c$  describes the critical porosity, below which flow is no longer possible and  $C$  is a geometrical factor. For a hexagonal arrangement of cylinders with periodic boundary conditions the critical porosity  $\phi_c$  equals  $1 - \pi/(2\sqrt{3})$  and the geometric factor  $C$  is  $16/(9\sqrt{6}\pi)$ .

The validation calculations were conducted in a 2D periodic domain, using a hexagonal arrangement of cylinders as depicted in Fig. 3. The cylinder radius was kept constant at 80 cells, while the area size was varied by increasing the x-direction edge length  $N_x$ . For the hexagonal arrangement, the y-direction edge length  $N_y$  was determined using the geometric relation  $N_y = \sqrt{3}N_x$ . Starting from  $N_x = 180$  cells, the area was successively increased and the resulting permeability was evaluated [29]. The results, along with a comparison of the Gebart equation and simulation results, are shown in Fig. 3. Additionally, it is worth noting that the fluid flow solver used in this work has undergone prior validation and comparison to experimental data in a separate publication. In said study [20], the solver was utilized to simulate the flow through a macro-porous polymer membrane and was compared to experimental results, indicating a favorable level of agreement between the simulation and the experiment.

In Fig. 4, an overview of the determination of all the structural characteristics is given.

## 2.3. Macroscopic flow model for wicking processes in LFAs

Lateral flow assays (LFAs) are easy-to-use medical diagnostic tests based on the self-sufficient transport of a liquid sample, containing analytes and detector particles, to a detection zone (test and control lines). One of the most popular LFAs are home pregnancy tests or the currently widespread COVID-19 rapid tests. The transport process is called wicking, which describes a surface-driven imbibition process in porous structures, where a non-wetting fluid (gas) is replaced by a wetting one (water), when subjected to a capillary suction pressure [30].

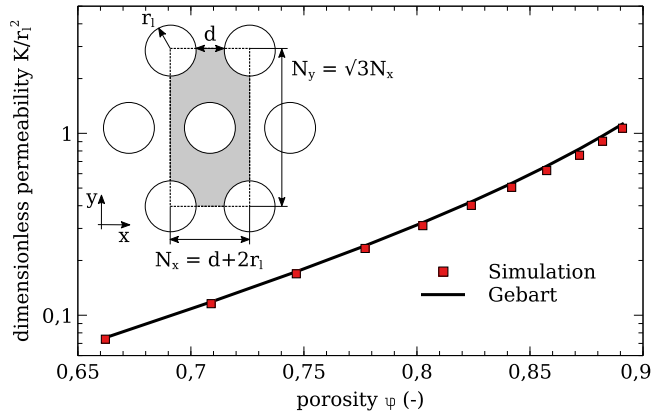


**Fig. 3.** The Stokes solver was validated by comparing its simulation results to the Gebart equation (5). The validation simulations were performed using a hexagonal arrangement, as schematically depicted where the gray rectangle represents the simulation domain.

In LFAs, the capillary-driven wicking process is realized by an open-pored and highly porous PPM as conductive medium. Thereby, the wicking process is significantly influenced by the morphology of the microstructure. The wicking time and the associated wicking velocity at the test and control line have a decisive influence on the sensitivity and thus on the test result [31].

Macroscopic flow models allow bridging the different length scales mentioned above. Thus, by using microstructural properties, the flow behavior on a macroscale can be predicted. The main approaches used to model the wicking process are all based on the description of the transport process, by including the dominant effects such as friction, gravity, and capillarity into the momentum balance equation. In this work, we only consider the horizontal flow behavior, which is why gravity can be neglected. Therefore, the prediction of wicking based on the balance of forces between a capillary and a viscous term is used:

$$\frac{2\gamma_{lg} \cos(\theta_e)}{r_{eff}} = \frac{\varphi}{K} \eta l \dot{l}. \quad (6)$$

Here,  $\gamma_{lg}$  describes the surface tension between the liquid and the air phase and  $\theta_e$  is the corresponding contact angle.  $r_{eff}$  represents the effective capillary radius, which is based on the mean pore radius  $r_c$  and a correction factor  $F(r_l, r_c)$ , as described in Eq. (2). The viscous term is described by the porosity  $\varphi$ , the permeability  $K$ , the viscosity  $\eta$ , the wicking length  $l$ , and the wicking velocity  $\dot{l}$ .

For the applied force balance, a fully analytical solution is given in [32] as follows:

$$l(t) = \sqrt{\frac{4\gamma_{lg} \cos(\theta_e)}{\eta} \frac{K}{\varphi r_{eff}}} \sqrt{t}. \quad (7)$$

By rearranging the previous Eq. (7), the wicking time  $t_w$  can be calculated in dependence of the permeability and the effective pore radius:

$$t_w = l^2 \cdot \frac{\varphi r_{eff}}{K} \cdot \frac{\eta}{4\gamma_{lg} \cos(\theta_e)} \quad (8)$$

For this investigation, the imbibition fluid was assumed to be pure water and the PPM was assumed to be a cellulose nitrate membrane (CN membrane). The properties listed in Table 1 are used for the following wicking predictions:

The surface tension  $\gamma_{lg}$  and the dynamic viscosity  $\eta$  for pure water are considered. The contact angle between the CN membrane and the liquid is taken from [33], where a contact angle between 40° and 60° was measured for pure water. Since the method presented here can be easily reproduced with the help of the presented workflows and equations, the focus of this work is not on the realistic mapping of

**Table 1**

Assumed wetting properties for an imbibition of pure water on a CN membrane liquid [33].

$\gamma_{lg}$ (mN m <sup>-1</sup> )	$\theta_e$ (°)	$\eta$ (mPa s)
72.0	50.0	1

the values, but on the presentation of the approach and its potential benefits for the accelerated development of novel membrane structures. Therefore, an average value of 50° is assumed for the static contact angle  $\theta_e$ .

#### 2.4. High-throughput workflow in Kadi4Mat

The described data-driven approach in Fig. 4 is realized by building and applying high-throughput data pipelines. For such purposes, the Karlsruhe Data Infrastructure for Material Science (Kadi4Mat) is being developed at the Karlsruhe Institute of Technology (Karlsruhe, Germany). The overall goal of Kadi4Mat is to provide a modular and generic architecture for handling large amounts of diverse research data from different disciplines and ultimately to accelerate research activities. Main components can be summarized as *Community Repository* [12] and *Electronic Lab Notebook (ELN)* [11]. While the community repository provides an extensive data sharing and managing infrastructure, the ELN enables the creation of reproducible and automatable workflows.

The workflow component mainly consists of a workflow editor which is based on an open source node editor library for Qt [34]. Within the framework of Kadi4Mat, there are two versions of this editor. One is a desktop-based, standalone software version called *KadiStudio*, while the second is a web-based version integrated into the web version of Kadi4Mat. In *KadiStudio*, the creation of workflows is implemented by adding and connecting nodes within a graphical user interface (GUI), each of the insertable nodes represents a specific process. The nodes can be divided into the following categories: (i) tool nodes that allow the integration of various programs or functions, (ii) environment nodes that provide different environments in which the tool nodes are executed, and finally (iii) built-in nodes that provide additional flexibility to the execution of a workflow. In particular, some of the built-in nodes that cover control mechanisms such as if-conditions and for-loops are fundamental to high-throughput automatable generation and analysis. Fig. 5 exemplifies the automated generation of porous membrane microstructures by three encapsulated for-loop nodes and a tool node that executes the generation process.

In order to connect *KadiStudio* to the Kadi4Mat repository, an application programming interface (API) is being developed that provides a set of functions for the interaction. The open source API can be integrated through the kadi-apy library [35], while the functions can be used as nodes in *KadiStudio*, as shown in Fig. 5.

When executing a workflow, the tool nodes used are translated into command line interface (CLI) commands, while the entire workflow is executed sequentially in a Linux terminal. A major advantage of the workflow editor is its technical nature of a graphical programming language, which makes it possible to make high-throughput research accessible to a wider range of users [11].

### 3. Results

#### 3.1. Data-driven structure linkages

In this study, a structure-wicking relationship is established between two microstructure parameters and the wicking time, using the designed workflows to generate and characterize microstructures. To calculate the wicking time using Eq. (8), the parameters ligament radius, pore radius, porosity, and permeability are required. To reduce the number of free structure variables, mathematical relationships were



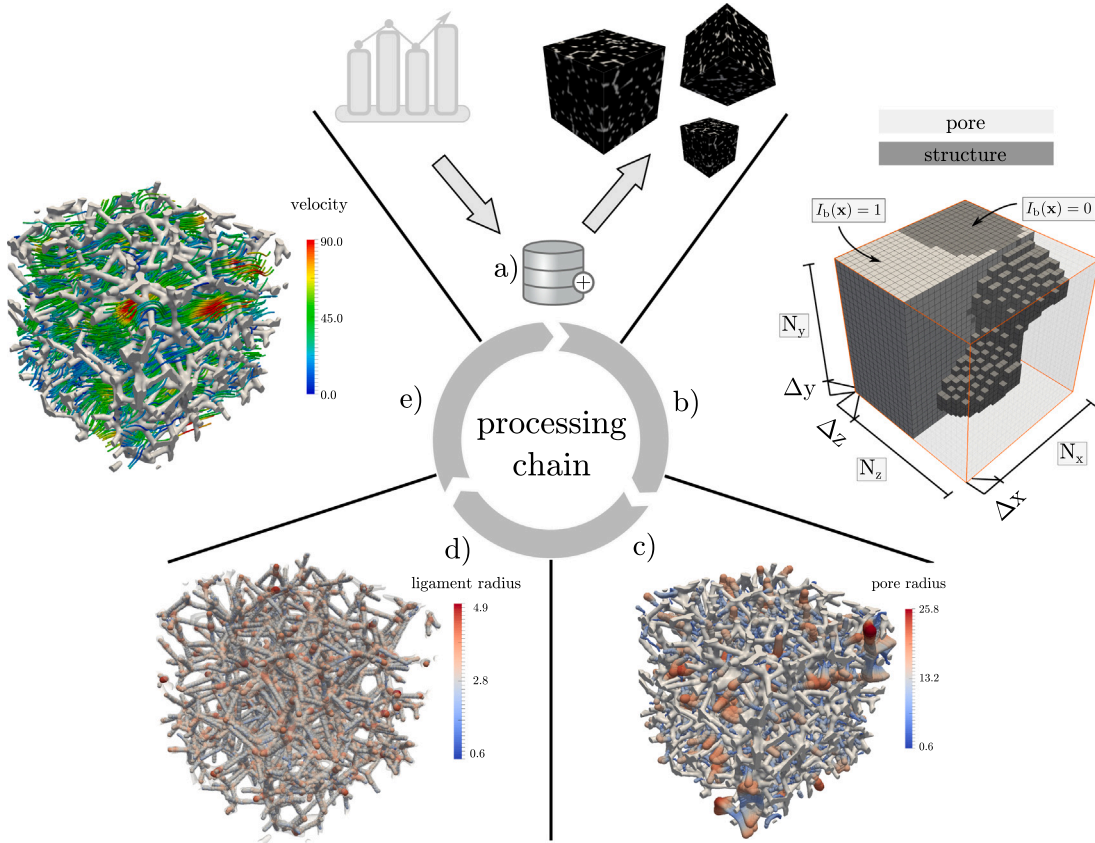


Fig. 4. Visualization of the abstract processing chain for obtaining the structure–property linkages. (a) Loading membrane microstructures from the database and storing the extracted characteristic properties in the database; (b) voxel-based determination of the porosity; (c) and (d) detection of the geometric pore and ligament radius in the porous microstructures; (e) fluid flow simulation for the permeability calculations. All characteristic properties are shown in dimensionless scales.

established for the remaining two parameters. In this study, the ligament radius and the porosity were chosen as the parameters of interest. It is worth mentioning that the influence of different combinations of two structure parameters can be explored by choosing different fit functions for the data. For the study, 407 structures were used as the database. Furthermore, by using this workflow and observing another property, any kind of structure–property relationship can be established.

### 3.1.1. Permeability as a function of porosity and mean ligament radius (Kozeny–Carman equation)

By performing fluid flow simulations in the pore space of the digital representations, the permeability  $K$  is determined as described in . Combining this with the extracted ligament radius  $r_l$  and the known porosity  $\phi$  yields a correlation expressed by the well-known Kozeny–Carman equation (K-C equation) [36]:

$$K(r_l, \phi) = \frac{\phi^3 r_l^2}{c(1 - \phi)^2}. \quad (9)$$

Here,  $c$  is a geometry factor that describes the shape of the pores and is obtained by a 3D fitting procedure, using the scientific graphics utility Gnuplot 5.2 [37]. Together with the fitted level, Fig. 6a shows the results of the fluid flow simulations for the structures with the porosities 83 %, 85 %, 87 %, and 89 %. As a result of the fitting procedure, it is found that the geometry factor  $c$  is determined to equal  $c = 15.7171$  for the investigated range of structural properties. For statistical validation, the coefficient of determination  $R^2$  was also calculated, where  $R^2$  corresponds to the value 0.966. This shows that the fitted Kozeny–Carman equation is an appropriate approximation to the data obtained.

### 3.1.2. Pore radius as a function of ligament radius and porosity

In a further step, we perform a linear regression procedure with the structural properties mean pore radius  $r_c$ , ligament radius  $r_l$ , and porosity  $\phi$ . Since the data showed a linear relationship in three-dimensional space, we chose the following approach function:

$$r_c(r_l, \phi) = d\phi + er_l + f. \quad (10)$$

By fitting the acquired data to Eq. (10), using the scientific graphics utility Gnuplot 5.2, we obtain the following parameters:  $d = 9.61415 \times 10^{-6}$  m,  $e = 3.17836$ , and  $f = -8.15231 \times 10^{-6}$  m. The coefficient of determination  $R^2$  has a value of 0.956, which proves that the chosen approach function in Eq. (10) is a suitable model. The data and the best-fit level of Eq. (10) are plotted in Fig. 6b.

### 3.2. Wicking time predictions in PPMs

Embedding the Eqs. (2), (9), and (10) into the macroscopic wicking model in Eq. (8) finally results in a correlation between the wicking time  $t_w$  and the structural properties porosity  $\phi$  and ligament radius  $r_l$ , as expressed in Eq. (11). There, the fitting parameters  $a$  and  $b$ , used to calculate an accurate effective capillary radius for open-pore structures, are taken from our previous work [18], which is described in more detail in . The fitting parameters  $c$ ,  $d$ ,  $e$ , and  $f$  were determined in the sections to establish a mathematical relationship for calculating permeability and pore radius in dependence of porosity and the ligament radius, respectively. The wetting properties are described by the surface tension  $\gamma_{lg}$ , the dynamic viscosity  $\eta$ , and the contact angle  $\theta_c$ , and are kept constant by the values described in Table 1. The remaining parameter  $l$  represents the desired wicking length.

Fig. 7a schematically illustrates the length scales to be bridged. The application scale is represented by the length of the test strip, while

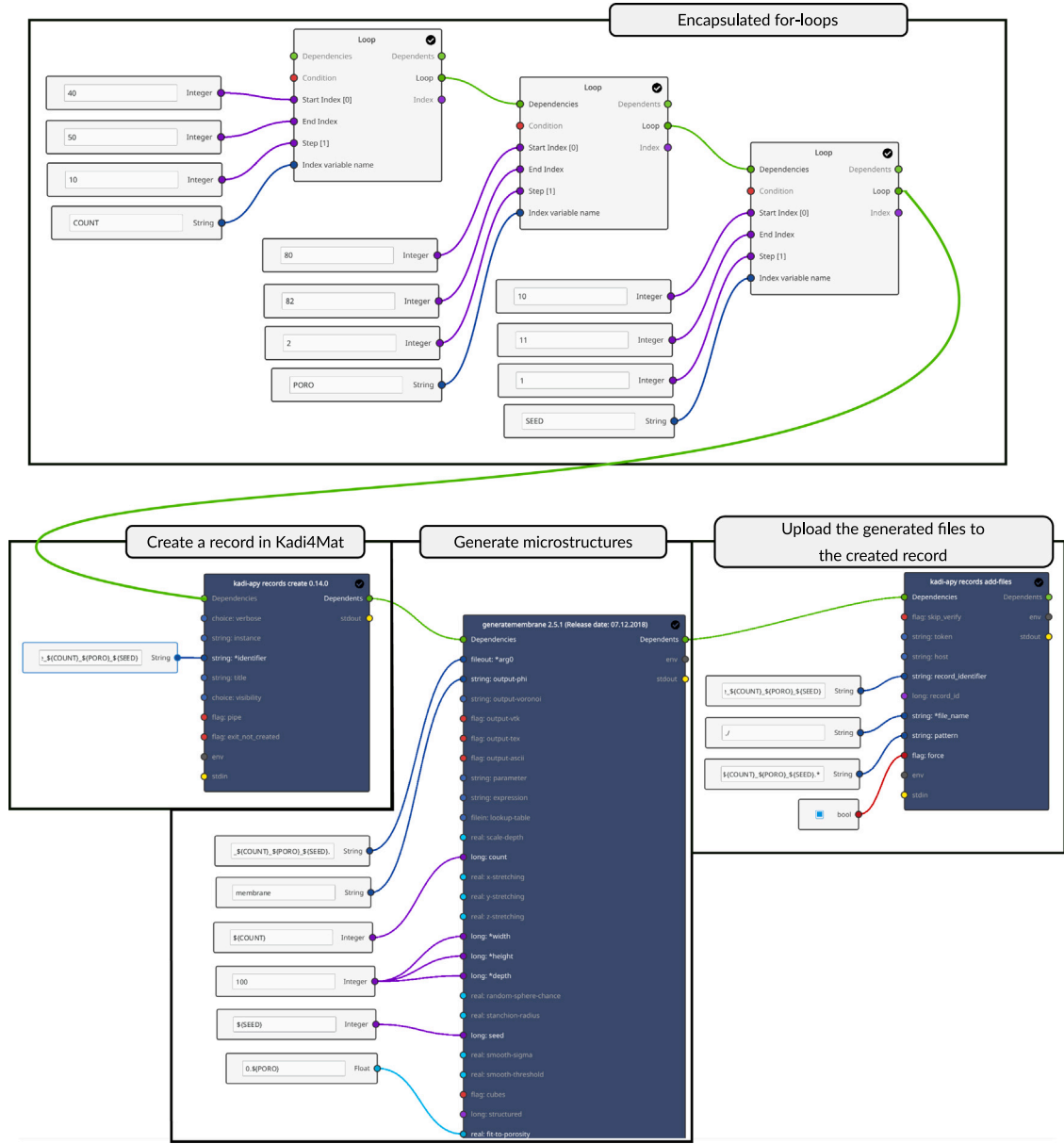


Fig. 5. Visualization of an applied workflow for the high-throughput structure generation. The workflow is realized with the *KadiStudio* workflow editor, while the boxes are added to highlight the executed steps.

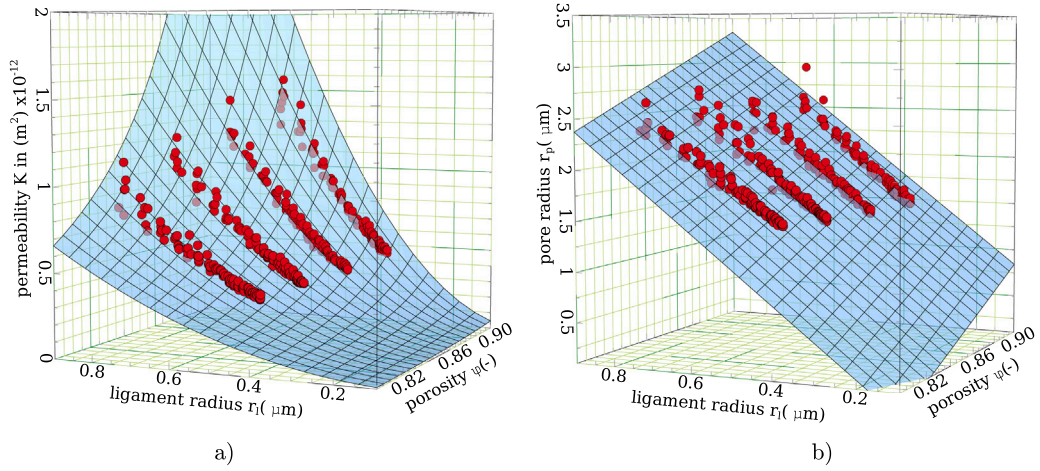
the microscale is described by the morphology of the microstructure (porosity  $\phi$ , ligament radius  $r_l$ , and pore radius  $r_c$ ). Thereby, a factor of 1000 has to be bridged.

$$t_w(r_l, \phi) = \frac{(d\phi + er_l + f)(ad\phi + (ae + b)r_l + af)(-1 + \phi)^2 c}{r_l^3 \phi^2} \cdot \frac{l^2 \mu}{4\gamma \cos(\theta_e)} \quad (11)$$

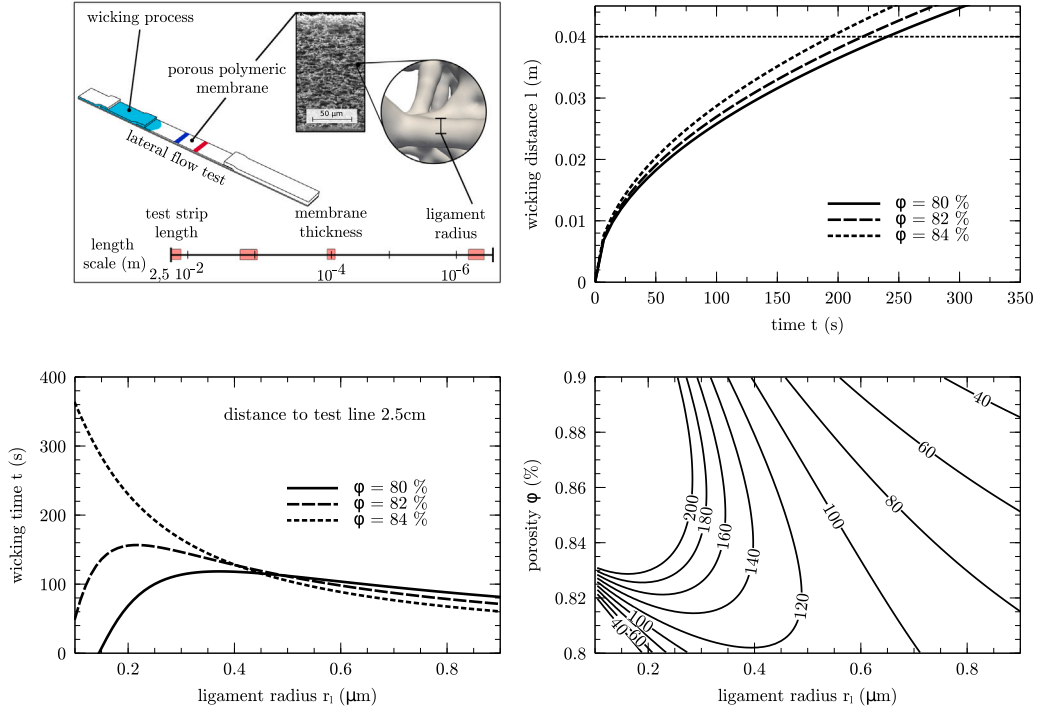
As a first proof of concept, Fig. 7b shows a typical wicking behavior in a graph where the wicking length  $l$  is plotted against the time  $t$ . Here, the curves follow the classical course, where the wicking behavior can be described in general terms with a root function  $l \sim t^{0.5}$  [38]. Here, the ligament radius for all three curves has the constant value  $r_l = 0.7 \mu\text{m}$  and the three porosities of 80 %, 82 %, and 84 % are shown. As can be seen in Fig. 6a and Fig. 6b, at a constant ligament radius, the pore radius and the permeability increase with an increasing porosity. In the three examples shown, this circumstance leads to a faster wicking behavior with increasing porosity.

Fig. 7c shows the wicking time for a wicking length of 0.025 m over the ligament radius, at three constant porosities. In contrast to Fig. 7b, no clear staggering of the wicking time can be seen, which is dependent on the porosity. Instead, structures with a higher porosity show a slower wicking behavior at smaller ligament radii, with this behavior tilting as the radius increases. This observation gives a first indication of the non-trivial relationship between the ligament radius, the porosity, and the wicking time.

A more general overview of the complex wicking behavior within the investigated property range is given by the contour plot in Fig. 7d. The wicking time is plotted as isochoric contour lines, as a function of the porosity and the ligament radius, while the wicking length is held constant as 0.025 m. As can be seen from Fig. 7c, the strong nonlinear correlation between the structural properties and the material behavior is first of all obvious. Second, there is no clear rule of thumb that summarizes the nonlinear behavior, since the trends linking structure to properties are highly dependent on the observed structural range. For instance, by assuming a constant porosity of 82 %, we can observe that



**Fig. 6.** (a) Flow simulation results: Correlation between the ligament radius  $r_l$  and the resulting permeability  $K$  of the porous membranes for different porosities, using the Kozeny–Carman equation. (b) Correlations between  $r_c$ ,  $r_l$  and  $\phi$ .



**Fig. 7.** Resulting plots for the wicking time prediction: (a) Overview of the application of the results, by using Eq. (11); (b) Wicking distance over wicking time, for different porosities and a constant ligament radius of  $0.7 \mu\text{m}$ ; (c) Wicking time over ligament radius, for different porosities; (d) Contour plot of isochores in (s), in dependence of the porosity and the ligament radius.

the wicking time increases when the ligament radius ranges from  $0.1 \mu\text{m}$  to  $0.2 \mu\text{m}$ , while it decreases when the ligament radius ranges from  $0.2 \mu\text{m}$  to  $0.9 \mu\text{m}$ . The isochores show that while different combinations of structural characteristics lead to different morphologies, the same wicking time can be achieved with an infinite number of different morphologies. This can be exploited in the design of LFTs, by maintaining the same wicking time along the isochores to simultaneously optimize the structural parameters for other requirements.

#### 4. Discussion

The presented results confirm that the influence of the morphologies ( $\phi$  and  $r_l$ ) on the wicking time and thus on the liquid velocity at the test and control line is immense. Since the flow velocity in the test area

has a crucial influence on the sensitivity of the test [39], it is important to know and predict the flow conditions, so as to improve and design highly sensitive LFAs [31]. The resulting correlation in Fig. 7d provides the necessary prediction for LFA design.

With respect to the virtual material design, the obtained structure–property linkage clarifies the relation between the structure and the resulting properties of the overall PSP chain relationship, according to which the PSP linkage has a many-to-one (forward model) and a one-to-many (inverse model) character [2]. In our case, this is shown by the fact that many structures can lead to a certain wicking time, which can be seen along the isochoric lines. Conversely, a certain wicking time can be realized by many structures, which can play a crucial role in the design of LFAs, since factors such as pore size have a further influence on the width of the test line [40] and thus on the sensitivity of the test.

Therefore, the test performance can be improved without changing the wicking behavior, by adapting the structure along the isochoric line.

## 5. Conclusion

In this work, 407 structures representing digital twins of porous polymeric membranes were generated by an algorithm. The characterization was done using fluid flow simulations and 3D image analysis methods. The obtained data was used to establish structural correlations by regression approaches that include the pore radius  $r_c$ , the ligament radius  $r_l$ , the porosity  $\phi$ , and the permeability  $K$ . Finally, using the determined structural relationships and a macroscopic wicking model, an isochoric diagram was created that analytically describes the complex relationship and allows a prediction of the wicking behavior. In order to follow the FAIR principles, the relationship was realized by implementing reusable workflows with the workflow editor *KadiStudio* and made available to the research community via Zenodo, as a public repository.

For future work, the created and provided workflows can easily be used to extend the characteristic ranges and apply them to new use cases. Moreover, not only digital twins of algorithmically generated membrane structures, but also time-dependent physical simulations of the underlying phase separation [24] or reconstructed membranes [20] could be additionally used. As a result, not only a structure–property relationship could be realized, but also a full process–structure–property relationship, which offers the possibility to tailor novel membranes more precisely, taking into account the manufacturing process, and thus improve the rapid adaptation of LFAs to new diseases.

## CRedit authorship contribution statement

**Willfried Kunz:** Conceptualization, Formal analysis, Methodology, Validation, Writing – original draft. **Patrick Altschuh:** Conceptualization, Data curation, Formal analysis, Visualization, Writing – original draft. **Marcel Bremerich:** Funding acquisition, Project administration, Writing – review & editing. **Michael Selzer:** Funding acquisition, Software, Data curation, Writing – review & editing. **Britta Nestler:** Funding acquisition, Resources, Supervision, Project administration, Writing – review & editing.

## Declaration of competing interest

The authors declare that they have no known competing financial interests or personal relationships that could have appeared to influence the work reported in this paper.

## Data availability

All acquired data points and created workflows are published on Zenodo <https://doi.org/10.5281/zenodo.7220573>, Ref. 41. To establish the described structure–property linkages, the software packages PACE3D, Gnuplot 5.2 [37], and *KadiStudio* were used. Thereby, the workflow editor *KadiStudio* [11] and the scientific graphic utility Gnuplot are openly accessible software. Although PACE3D is a licensed software package, all algorithms used by PACE3D are already published. To reproduce the generation and characterization workflow published here, either a PACE3D license can be acquired, the algorithms used can be reproduced on the basis of the cited algorithms, or individual tools can be replaced with your own available software and integrated into the workflows, instead of the PACE3D software.

## Acknowledgments

This work was mainly supported by the German government, through the BMBF project Multipore, Germany (project ID: 13FH020KX0), by Sartorius Stedim Biotech GmbH in Goettingen, Germany, and by the Ministry of Science, Research and Arts Baden-Württemberg, Germany (MWK-BW), in the project MoMaF–Science Data Center, with funds from the state digitization strategy digital@bw, Germany (project number 57). Furthermore, we would like to thank the Helmholtz Association, Germany for partially funding the development of Kadi4Mat through the program “MTET: 38.04.04”.

## References

- [1] L. Himanen, A. Geurts, A.S. Foster, P. Rinke, Data-driven materials science: status, challenges, and perspectives, *Adv. Sci.* 6 (21) (2019) 1900808.
- [2] A. Agrawal, A. Choudhary, Perspective: Materials informatics and big data: Realization of the “fourth paradigm” of science in materials science, *Appl. Mater.* 4 (5) (2016) 053208.
- [3] N. Romanos, M. Kalogerini, E.P. Koumoulos, A. Morozinis, M. Sebastiani, C. Charitidis, Innovative Data Management in advanced characterization: Implications for materials design, *Mater. Today Commun.* 20 (2019) 100541.
- [4] S.R. Kalidindi, M. Buzzy, B.L. Boyce, R. Dingreville, Digital twins for materials, *Front. Mater.* (2022) 48, <http://dx.doi.org/10.3389/fmats.2022.818535>.
- [5] M. Röding, E. Schuster, K. Logg, M. Lundman, P. Bergström, C. Hanson, T. Gebäck, N. Lorén, Computational high-throughput screening of fluid permeability in heterogeneous fiber materials, *Soft Matter* 12 (29) (2016) 6293–6299.
- [6] C. Gao, X. Min, M. Fang, T. Tao, X. Zheng, Y. Liu, X. Wu, Z. Huang, Innovative materials science via machine learning, *Adv. Funct. Mater.* 32 (1) (2022) 2108044, <http://dx.doi.org/10.1002/adfm.202108044>.
- [7] I.G. Clayson, D. Hewitt, M. Hutereau, T. Pope, B. Slater, High throughput methods in the synthesis, characterization, and optimization of porous materials, *Adv. Mater.* 32 (44) (2020) 2002780.
- [8] R. Bostanabad, Y. Zhang, X. Li, T. Kearney, L.C. Brinson, D.W. Apley, W.K. Liu, W. Chen, Computational microstructure characterization and reconstruction: Review of the state-of-the-art techniques, *Prog. Mater. Sci.* 95 (2018) 1–41.
- [9] S. Curtarolo, G.L. Hart, M.B. Nardelli, N. Mingo, S. Sanvito, O. Levy, The high-throughput highway to computational materials design, *Nature Mater.* 12 (3) (2013) 191–201.
- [10] M.D. Wilkinson, M. Dumontier, I.J. Aalbersberg, G. Appleton, M. Axton, A. Baak, N. Blomberg, J.-W. Boiten, L.B. da Silva Santos, P.E. Bourne, et al., The FAIR Guiding Principles for scientific data management and stewardship, *Sci. Data* 3 (1) (2016) 1–9.
- [11] L. Griem, P. Zschumme, M. Laqua, N. Brandt, E. Schoof, P. Altschuh, M. Selzer, *KadiStudio: FAIR modelling of scientific research processes*, *Data Sci. J.* 21 (1) (2022) 16, <http://dx.doi.org/10.5334/dsj-2022-016>.
- [12] N. Brandt, L. Griem, C. Herrmann, E. Schoof, G. Tosato, Y. Zhao, P. Zschumme, M. Selzer, *Kadi4Mat: A research data infrastructure for materials science*, *Data Sci. J.* 20 (1) (2021) 8, <http://dx.doi.org/10.5334/dsj-2021-008>.
- [13] P. Altschuh, *Skalenübergreifende Analyse Makroporöser Membranen Im Kontext Digitaler Zwillinge* (Ph.D. thesis), Karlsruhe Institute of Technology, Karlsruhe, 2020, <http://dx.doi.org/10.5445/IR/1000122904>.
- [14] F. Wang, P. Altschuh, L. Ratke, H. Zhang, M. Selzer, B. Nestler, Progress report on phase separation in polymer solutions, *Adv. Mater.* 31 (26) (2019) 1806733, <http://dx.doi.org/10.1002/adma.201806733>.
- [15] M. Stucki, M. Loepe, W.J. Stark, Porous polymer membranes by hard templating—a review, *Adv. Eng. Mater.* 20 (1) (2018) 1700611.
- [16] M. Ulbricht, Advanced functional polymer membranes, *Polymer* 47 (7) (2006) 2217–2262.
- [17] J. Rouquerol, D. Avnir, C.W. Fairbridge, D.H. Everett, J. Haynes, N. Pernicone, J.D. Ramsay, K.S.W. Sing, K.K. Unger, Recommendations for the characterization of porous solids (Technical Report), *Pure Appl. Chem.* 66 (8) (1994) 1739–1758.
- [18] P. Altschuh, W. Kunz, M. Bremerich, A. Reiter, M. Selzer, B. Nestler, Wicking in porous polymeric membranes: Determination of an effective capillary radius to predict the flow behavior in lateral flow assays, *Membranes* 12 (7) (2022) <http://dx.doi.org/10.3390/membranes12070638>.
- [19] S. Bargmann, B. Klusemann, J. Markmann, J.E. Schnabel, K. Schneider, C. Soyarslan, J. Wilmers, Generation of 3D representative volume elements for heterogeneous materials: A review, *Prog. Mater. Sci.* 96 (2018) 322–384, <http://dx.doi.org/10.1016/j.pmatsci.2018.02.003>.
- [20] A. Ley, P. Altschuh, V. Thom, M. Selzer, B. Nestler, P. Vana, Characterization of a macro porous polymer membrane at micron-scale by Confocal-Laser-Scanning Microscopy and 3D image analysis, *J. Membr. Sci.* 564 (2018) 543–551, <http://dx.doi.org/10.1016/j.memsci.2018.07.062>.
- [21] P. Altschuh, Y.C. Yabansu, J. Hötzer, M. Selzer, B. Nestler, S.R. Kalidindi, Data science approaches for microstructure quantification and feature identification in porous membranes, *J. Membr. Sci.* 540 (2017) 88–97, <http://dx.doi.org/10.1016/j.memsci.2017.06.020>.



- [22] L. Wallat, P. Altschuh, M. Reder, B. Nestler, F. Poehler, Computational design and characterisation of gyroid structures with different gradient functions for porosity adjustment, *Materials* 15 (10) (2022) 3730, <http://dx.doi.org/10.3390/ma15103730>.
- [23] A. August, J. Ettrich, M. Rölle, S. Schmid, M. Berghoff, M. Selzer, B. Nestler, Prediction of heat conduction in open-cell foams via the diffuse interface representation of the phase-field method, *Int. J. Heat Mass Transfer* 84 (2015) 800–808, <http://dx.doi.org/10.1016/j.ijheatmasstransfer.2015.01.052>.
- [24] F. Wang, L. Ratke, H. Zhang, P. Altschuh, B. Nestler, A phase-field study on polymerization-induced phase separation occasioned by diffusion and capillary flow—a mechanism for the formation of porous microstructures in membranes, *J. Sol-Gel Sci. Technol.* (2020) 1–19, <http://dx.doi.org/10.1007/s10971-021-05565-3>.
- [25] H. Zhang, Y. Wu, F. Wang, F. Guo, B. Nestler, Phase-field modeling of multiple emulsions via spinodal decomposition, *Langmuir* 37 (17) (2021) 5275–5281, <http://dx.doi.org/10.1021/acs.langmuir.1c00275>.
- [26] J. Hötzer, A. Reiter, H. Hierl, P. Steinmetz, M. Selzer, B. Nestler, The parallel multi-physics phase-field framework Pace3D, *J. Comput. Sci.* 26 (2018) 1–12, <http://dx.doi.org/10.1016/j.jocs.2018.02.011>.
- [27] F. Aurenhammer, Voronoi diagrams—a survey of a fundamental geometric data structure, *ACM Comput. Surv.* 23 (3) (1991) 345–405, <http://dx.doi.org/10.1145/116873.116880>.
- [28] B.R. Gebart, Permeability of unidirectional reinforcements for RTM, *J. Compos. Mater.* 26 (8) (1992) 1100–1133.
- [29] A. Nabovati, E.W. Llewellyn, A.C. Sousa, A general model for the permeability of fibrous porous media based on fluid flow simulations using the lattice Boltzmann method, *Composites A* 40 (6–7) (2009) 860–869.
- [30] R. Masoodi, K.M. Pillai, *Wicking in Porous Materials: Traditional and Modern Modeling Approaches*, CRC Press, Boca Raton, FL, 2012.
- [31] F. Jamshidi, W. Kunz, P. Altschuh, M. Bremerich, R. Przybylla, M. Selzer, B. Nestler, Geometric flow control in lateral flow assays: Macroscopic single-phase modeling, *Phys. Fluids* 34 (2022) 062110, <http://dx.doi.org/10.1063/5.0093316>.
- [32] N. Fries, D. Quéré, *Capillary Transport Processes in Porous Materials-Experiment and Model*, Cuvillier Verlag, Göttingen, GER, 2010.
- [33] S. a Zhdanov, V.M. Starov, V.D. Sobolev, M.G. Velarde, Spreading of aqueous SDS solutions over nitrocellulose membranes, *J. Colloid Interface Sci.* (ISSN: 0021-9797) 264 (2003) 481–489, [http://dx.doi.org/10.1016/S0021-9797\(03\)00520-4](http://dx.doi.org/10.1016/S0021-9797(03)00520-4), URL <http://www.ncbi.nlm.nih.gov/pubmed/16256668>.
- [34] D.P. et al, Qt5 node editor, 2017, <https://github.com/paceholder/nodeeditor>.
- [35] Kadi4Mat Team and Contributors, IAM-CMS/Kadi-Apy: Kadi4Mat API Library, Zenodo, 2022, <http://dx.doi.org/10.5281/zenodo.6623518>.
- [36] K. Xu, W. Wei, Y. Chen, H. Tian, S. Xu, J. Cai, A pore network approach to study throat size effect on the permeability of reconstructed porous media, *Water* 14 (1) (2022) 77, <http://dx.doi.org/10.3390/w14010077>.
- [37] T. Williams, C. Kelley, C. Bersch, H.-B. Bröker, J. Campbell, R. Cunningham, D. Denholm, G. Elber, R. Fearick, C. Grammes, et al., gnuplot 5.2, in: *An Interactive Plotting Program*, Vol. 2, 2017, Available Online: [http://www.gnuplot.info/docs\\_5](http://www.gnuplot.info/docs_5).
- [38] M. Boodaghi, A. Shamloo, A comparison of different geometrical elements to model fluid wicking in paper-based microfluidic devices, *AIChE J.* 66 (1) (2020) e16756.
- [39] M.A. Mansfield, Nitrocellulose membranes for lateral flow immunoassays: A technical treatise, *Lateral Flow Immunoassay* (2009) 1–19.
- [40] G.A. Posthuma-Trumpie, J. Korf, A. van Amerongen, Lateral flow (immuno) assay: its strengths, weaknesses, opportunities and threats. A literature survey, *Anal. Bioanal. Chem.* 393 (2) (2009) 569–582.
- [41] W. Kunz, P. Altschuh, M. Bremerich, M. Selzer, B. Nestler, Source Data Belonged to "Establishing Structure-Property Linkages for Wicking Time Predictions in Porous Polymeric Membranes Using a Data-Driven Approach", Zenodo, 2022, <http://dx.doi.org/10.5281/zenodo.7220573>, Zenodo.